



Controlled treatment of a high velocity anisotropic aquifer model contaminated by hexachlorocyclohexanes

Iheb Bouzid, Julien Maire, Fabien Laurent, Mathias Broquaire, Nicolas Fatin-Rouge

► To cite this version:

Iheb Bouzid, Julien Maire, Fabien Laurent, Mathias Broquaire, Nicolas Fatin-Rouge. Controlled treatment of a high velocity anisotropic aquifer model contaminated by hexachlorocyclohexanes. *Environmental Pollution*, 2021, 268, pp.115678. 10.1016/j.envpol.2020.115678 . hal-02962730

HAL Id: hal-02962730

<https://hal.science/hal-02962730>

Submitted on 17 Oct 2022

HAL is a multi-disciplinary open access archive for the deposit and dissemination of scientific research documents, whether they are published or not. The documents may come from teaching and research institutions in France or abroad, or from public or private research centers.

L'archive ouverte pluridisciplinaire **HAL**, est destinée au dépôt et à la diffusion de documents scientifiques de niveau recherche, publiés ou non, émanant des établissements d'enseignement et de recherche français ou étrangers, des laboratoires publics ou privés.



Distributed under a Creative Commons Attribution - NonCommercial 4.0 International License

Controlled treatment of a high velocity anisotropic aquifer model contaminated by hexachlorocyclohexanes

Iheb Bouzid ^a, Julien Maire ^a, Fabien Laurent ^b, Mathias Broquaire ^c, Nicolas Fatin-Rouge ^{a*}

^a Université de Bourgogne Franche-Comté–Besançon, Institut UTINAM–UMR CNRS 6213, 16, route
de Gray, 25030, Besançon, France

^b SOLVAY, Centre de Recherche et Innovation de Lyon, DRP-ERA, 85 rue des Frères Perret 69192 Saint
Fons

^c SOLVAY, Direction Réhabilitation Environnement, Parc Everest, 54 rue Marcel Dassault 69740
Genas

** Corresponding author, nicolas.fatin-rouge@univ-fcomte.fr*

Color is not required in print.

Abstract:

Xanthan gels were assessed to control the reductive dechlorination of hexachlorocyclohexanes (HCHs) and trichlorobenzenes (TCBs) in a strong permeability contrast and high velocity sedimentary aquifer. An alkaline degradation was selected because of the low cost of NaOH and Ca(OH)₂. The rheology of alkaline xanthan gels and their ability to deliver alkalinity homogeneously, while maintaining the latter, were studied. Whereas the xanthan gels behaved like non-Newtonian shear-thinning fluids, alkalinity and Ca(OH)₂ microparticles had detrimental effects, yet, the latter decreased with the shear-rate. Breakthrough curves for the NaOH and Ca(OH)₂ in xanthan solutions, carried out in the lowest permeability soil (9.9 μm²), demonstrated the excellent transmission of alkalinity, while moderate pressure gradients were applied. Injection velocities ranging from 1.8 to 3.8 m.h⁻¹ are anticipated in the field, given the permeability range from 9.9 to 848.7 μm². Despite a permeability contrast of 8.7 in an anisotropic aquifer model, the NaOH and the Ca(OH)₂ both in

xanthan gels spread only 5- and 7-times faster in the higher permeability zone, demonstrating that the delivery was enhanced. Moreover, the alkaline gels which were injected into a high permeability layer under lateral water flow, showed a persistent blocking effect and longevity (timescale of weeks), in contrast to the alkaline solution in absence of xanthan. Kinetics of alkaline dechlorination carried out on the historically contaminated soil, using the $\text{Ca}(\text{OH})_2$ suspension in xanthan solution, showed that HCHs were converted in TCBs by dehydrodechlorination, whereas the latter were then degraded by reductive hydrogenolysis. Degradation kinetics were achieved within 30 h for the major and most reactive fraction of HCHs.

Capsule: *In situ* remediation of a high velocity anisotropic aquifer historically contaminated by hexachlorocyclohexanes was assessed using alkaline reagents delivered in xanthan solutions

1. Introduction

Groundwater (GW) is an essential resource for drinking water production, because of its proximity and the purifying processes that occur during percolation [1,2]. In France, 96% of the catchments for drinking water industry are from GW, whereas this represents 66% of volumes [3]. Besides, GW also feeds natural ecosystems, whose health depends on its quality. GW quality has worsened, since anthropic pressure increased on that resource and because of contaminations from various origins.

In France, three-quarters of the soil and water pollution events involve organic compounds, among which chlorinated organic compounds (COCs) represent the majority [4]. Former industrial activities have engendered some major and persistent pollution issues. Lindane (γ -hexachlorocyclohexane) production and its use as a pesticide, was among the most impacting practices, because about 450000 tons of this highly toxic and bioaccumulating molecule were used worldwide between 1950 and 2000 [5–8]. This molecule and some of its seven hexachlorocyclohexane (HCH) isomers are part of the persistent organic pollutant list, because α , β and δ isomers were co-produced by 70 to 90% [9–11]. Indeed, HCHs are unfortunately carcinogenic and detrimental to the nervous and to the endocrine systems [12]. Besides the background HCH-contamination, hot spots are found all over Europe, because of former production units or warehouses. Because of their toxicity, low water solubility and vapor pressure, HCHs remain in soils for decades [10]. There, they feed plumes of dissolved pollutants, causing the long-term quality degradation of water contacting them.

In E.U., the water framework directive 2000/60/EC aims at the short-term recovery of good ecological status of natural water. The *in situ* remediation (ISR) of contaminated soils is growing, because it reduces the risks associated to contaminants dissemination and hazards [13]. Moreover, this strategy is especially advised when the access to contaminants is hindered, e.g. because of depth. Yet, ISR may be very technical in challenging situations, where underground heterogeneity and anisotropy hinder the access to contaminants. In particular, it is acknowledged that strong permeability contrasts hinder the homogeneous delivery of remediation fluids that mainly sweep through the

most permeable pathways [14–16]. Soil anisotropy leads to uncontrolled radii of influence (ROI), preferential flows and the heterogeneous distribution of amendments [17–23]. Thus, low permeability zones where contaminants are often trapped are badly swept and remain untreated. Besides the rise of costs for remediation, several effects like back diffusion tailing and rebound are often observed, which hinder the lasting recovery of GW quality due to ineffective treatments [24].

Fighting the fingering of injected fluids requires to increase their capillary number [25,26]. This well-known trouble led to the use of viscous, but shear-thinning fluids in oil recovery [14,27–30]. These behaviors, observed for associative polymers like xanthan and for foams, are used for the ISR of contaminated soils [20,21,23,31–42].

Fortunately, several means exist to remove HCH, among which chemical degradation is especially suitable for low to medium range contaminant concentrations [12,43–45]. *In situ* dechlorination via chemical reduction is often suitable for the degradation of COCs in the underground, because of the low concentrations of oxidizing molecules. Despite the fact that many studies have highlighted the interest of nano-zero-valent iron (nZVI), obvious barriers raised, such as cost, persistence, and health concerns [46–48]. Besides, alkaline degradation of HCHs could be a cheaper alternative [10,48,49]. It might be beneficial for the environment because of the lower toxicity of degradation products [44,49]. Yet, one should use carefully alkaline reagents like quicklime, since they may engender hazardous reactions and metabolites [50,51]. Half-lives for the alkaline degradation (pH=11.7) of most HCHs dissolved in ethanol/water mixtures are reported to range from 0.5 to 1h at 20°C [52]. However, hydrophobic HCHs desorb slowly from soils and require persistent action, especially in high velocity aquifers [24]. There, an aqueous $\text{Ca}(\text{OH})_2$ suspension could be a long-lasting reagent to maintain alkalinity, considering its delayed dissolution.

This paper reports a laboratory study about a high velocity and strongly heterogenous aquifer contaminated by HCHs and trichlorobenzenes (TCBs). In that challenging situation, the control of amendment delivery and the continued blocking of GW flow in the treated zone are critical for the

86 achievement of the remediation. Therefore, the study aims at assessing the performances of xanthan
87 solutions to deliver persistent alkali in strong permeability-contrasted aquifers and maintaining their
88 action. It also provides accurate information on kinetics of COCs degradation involved in the
89 remediation of the contaminated aquifer.

90

2. Materials and methods

2.1 Contaminated soils

The studied soil was collected using non-destructive sonic core sampling at a former lindane production facility. Site characterization shown the contaminated aquifer was strongly heterogeneous, with no geological continuity, and cm to m-scale variations. In addition, no correlation was evidenced between contamination and soil permeability. Spatial size distribution of soil particles was characterized by sieving [53]. Three model soil fractions (fine sand, medium sand and coarse sand) having D_{10} - D_{90} of 54-600, 160-600 and 80-2100 μm , respectively, were obtained through sieving. D_{10} and D_{90} correspond to the 10th and 90th percentile of grain size distribution, respectively. Permeabilities (k) of the model soils were 9.9, 96.7 and 848.7 μm^2 , respectively, as measured using the constant head technique [54]. These permeabilities were mainly chosen to recreate permeability contrasts in sandboxes closer to those measured from soil cores. The porosities of the materials were 0.32 for the fine and medium sands and 0.34 for the coarse one. Porosity was measured by weighing a column before and after filling it with water to determine the porous volume (PV) of the soil sample [55]. Given the complex contamination generated by lindane production, the fine sand (9.9 μm^2) was characterized by the concentrations of the detected contaminants, namely α , β , γ and δ -HCH isomers, and 1,2,3 and 1,2,4-TCB isomers. The contaminated soils were collected in sealed flasks and stored upside-down to avoid contaminants volatilization.

2.2 Chemicals

Xanthan gum (Rhodicare) was supplied by SOLVAY in the form of a dry powder. Xanthan solutions were prepared by dispersing the required amount of solid polymer in deionized water. The suspensions were heated (70°C) under stirring for 45 min. until the solubilization of the polymer and the achievement of a clear solution. Sodium hydroxide (> 97%, Fisher) and calcium chloride (98%, Prolabo) were used to prepare aqueous $\text{Ca}(\text{OH})_2$: NaOH and CaCl_2 were directly solubilized in two 0.2% xanthan solutions to a concentration of 0.6% corresponding to a $\text{Ca}(\text{OH})_2$ concentration of 0.3%

after mixing the two solutions. Finally, the resulting Ca(OH)_2 suspension in xanthan solution was dispersed using a high-performance dispersing instrument at 25000 rpm for 3 min. (ultra-turrex®, IKA T25). The obtained fluid was not filtered before injection. The Ca(OH)_2 microparticles obtained were characterized by optical microscopy (Nachet 300) and had an average size of $8 \pm 2 \mu\text{m}$. Eosin (Acros Organics) was used to color the circulating water in the sandbox, mimicking the natural GW flow. Phenolphthalein and sulfuric acid (Fisher) were used for the acid-base determination of alkalinity. The universal indicator (Fisher) was chosen to monitor pH changes of the injected alkaline fluids in sandbox. Acetone (>99%, Fisher) and n-hexane (95%, Fisher) were used as solvents to extract the contaminants from soils. 1,2,4-TCB (99%), 1,2,3-TCB (99%), 1,3,5-TCB (98%), 1,2-dichlorobenzene (DCB, 98%), 1,3-DCB (98%), 1,4-DCB (>99%), chlorobenzene (CB, 99%) were obtained from Alfa Aesar. A solution containing a mixture of HCH isomers (Fisher) and benzene (99%, Janssen Chemica) was used for the standards preparation in methanol (>99%, Fisher).

2.3 Bulk viscosity measurements

Bulk rheological characterization of the xanthan solutions was performed using a rotational rheometer (Malvern Kinexus pro+) equipped with a cone-plate measuring system. Rheological measurements were carried out at 25°C. Eighty measurement points were repeated 4-times for each solution.

2.4. Alkalinity transport and experimental set-up

The rheological behavior of injected alkaline (NaOH 0.1% M and Ca(OH)_2 at 0.3%) xanthan-based fluids through porous medium were performed in columns (l: 0.1 to 0.4 m, i.d.: 3.2 cm, PV = 56 mL) and in sandboxes (dim.: 2×18×25 cm, PV = 276 mL). The experimental set-up is illustrated in Figure 1. The soils were packed wet and gently vibrated to ensure a uniform packing.

The fine and coarse materials ($k = 9.9$ and $848.7 \mu\text{m}^2$) were used in the columns experiments. The sandbox was filled under water with medium and coarse sands ($k = 96.7$ and $848.7 \mu\text{m}^2$) to make a representative elementary volume (REV) and an average permeability contrast of 8.7, as deduced

from the site characterization. The soil was held at the top of the sandbox by a rigid plate. The water circulation simulating the GW flow was injected with a peristaltic pump (Masterflex) connected to a water tank and to a perforated tube (HDPE, d.: 2 cm) placed on the left side of the sandbox. The average water circulation rate was 10 m.d⁻¹. The recovery of water flowing through the sandbox was performed using a second perforated tube at the right end. The water recovered from this second well was collected into another glass flask. The reagent solutions were injected through an opening at the back center of the sandbox (Fig. 1).

The reagent solutions were maintained under mechanical agitation (600 rpm) and they were injected using a dosing pump (KNF Simdos 10). The pressures were recorded automatically with an automate (Arduino Uno) connected to a computer.

The apparent viscosities of the injected solutions were measured in columns from pressure drops at Darcy flow rates of 1.98×10^{-4} , 3.96×10^{-4} , 6.60×10^{-4} and 10.6×10^{-4} m.s⁻¹.

The alkalinity breakthrough curves were carried out in columns (l: 0.1 to 0.4 m, i.d.: 3.2 cm) filled with fine sand (9.9 μm²). The alkaline xanthan solutions were injected at a rate of 6.60×10^{-4} m.s⁻¹. The alkalinity of the recovered effluent was monitored by sulfuric acid titration. The reference value was the alkalinity of the fluids before injection. A total of 9 PVs were injected. Breakthrough curves were obtained by plotting the ratio of the alkaline concentration C measured in the effluent at time t and the one of the injected fluid C_0 , vs. time. The estimation of the Darcy velocity u (m.s⁻¹) and of the tracers dispersivity α (m) is possible using the solution of the advection-dispersion equation in semi-infinite column [56]:

$$\frac{C}{C_0} = 0.5 \cdot \left[\operatorname{erfc} \left(\frac{x-ut}{\sqrt{4 \cdot \alpha \cdot u \cdot t}} \right) + \exp \left(\frac{x \cdot u}{D} \right) \cdot \operatorname{erfc} \left(\frac{x+ut}{\sqrt{4 \cdot \alpha \cdot u \cdot t}} \right) \right] \quad (1)$$

where x (m) is the length of the column and D (m².s⁻¹) is the dispersion coefficient.

When x/α is large, the second term can be neglected and the eq. 1 becomes:

$$\frac{c}{c_0} \sim 0.5 \cdot \operatorname{erfc} \left(\frac{x-ut}{\sqrt{4\alpha u t}} \right) \quad (1')$$

Values of u and α were fitted from the breakthrough curve for the NaOH in xanthan solution assuming that it was a small conservative tracer. Then setting the obtained α -value, the retardation factor for the $\text{Ca}(\text{OH})_2$ suspension in xanthan solution was calculated as the ratio of the Darcy velocities fitted from the NaOH and the $\text{Ca}(\text{OH})_2$ breakthrough curves, respectively. Besides, considering some irreversible trappings of $\text{Ca}(\text{OH})_2$ particles, a transmission factor was calculated from the plateaus-value of the C/C_0 ratio at long times, assuming a steady-state regime.

At the end of the transport experiments, the column was sacrificed for the evaluation of spatial distribution of alkalinity. The column was dissected into 20 segments of 2 cm and the soil alkalinity was measured in each section to better assess the $\text{Ca}(\text{OH})_2$ transport. The collected soil fractions were placed in a beaker containing 20 mL of pure water. Then, some drops of phenolphthalein were added, before the alkalinity was titrated under agitation with sulfuric acid.

The alkaline xanthan-based fluids injected into the sandbox were colored by the universal pH indicator (purple color at pH 12). The universal indicator (0.05%w) allowed the visualization of the solutions propagation and the observation of possible pH changes in the treated area over time. The injection of alkaline solutions in the most permeable layer was stopped when the edges of the sandbox were reached.

181

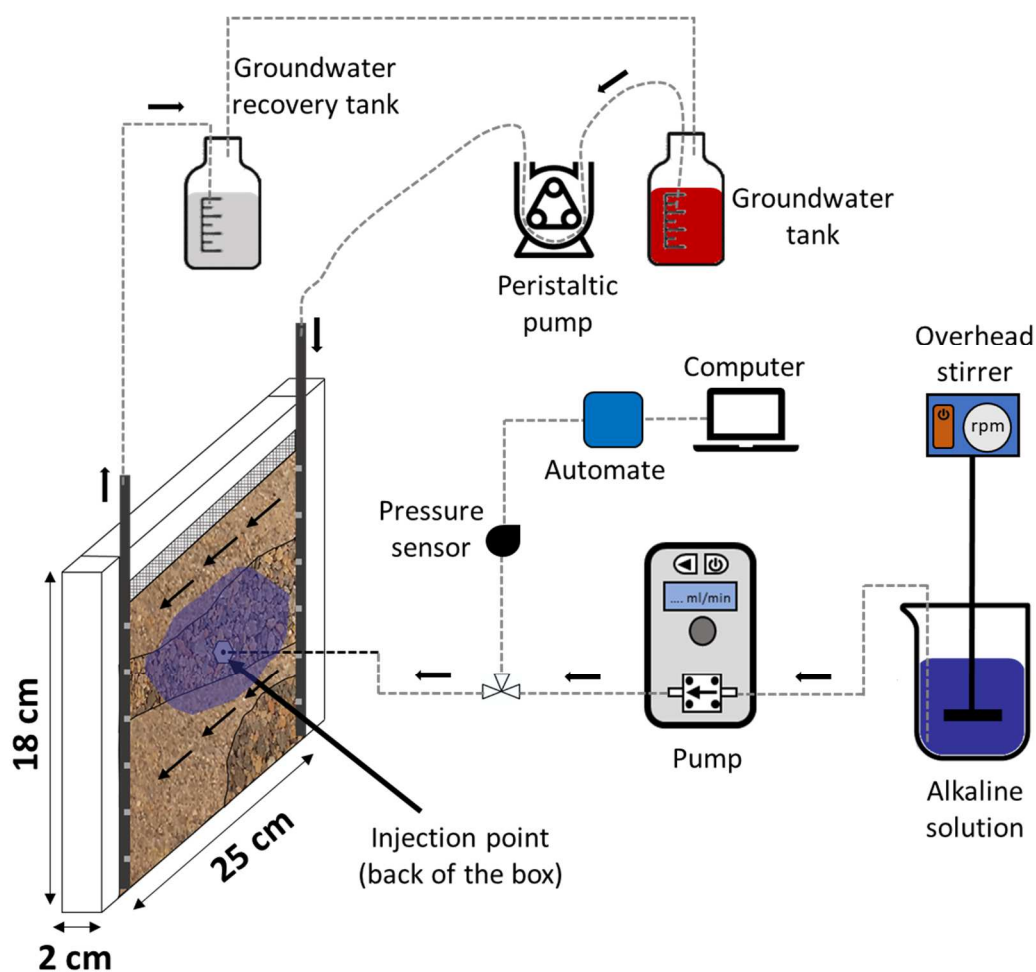


Figure 1. Experimental set-up used for the injections of solutions.

2.5 Kinetics of contaminants degradation

The kinetic study of HCH and TCB degradation was carried out in short columns (l: 5 cm, i.d.: 3.2 cm). Each column was prepared with approximately 60 g of fine sand from the contaminated site. For each column, 1 PV of xanthan solution (0.2%) carrying $\text{Ca}(\text{OH})_2$ (0.3%, pH 12) was injected. The reaction was monitored at 20°C for 72h. Columns were sacrificed at different times for the analysis of HCH and TCB concentrations. The untreated soil was used as a reference for initial contaminant concentrations. The experiments were duplicated, and the averaged results were used.

The kinetics of HCH disappearance was pseudo first-order. The kinetic constants (h^{-1}) for HCH were obtained by non-linear fitting of concentrations vs. time. TCBs kinetic constants were obtained by fitting their concentrations using eq. 2:

$$C = \frac{k_1 C_0}{k_2 - k_1} (e^{-k_1 t} - e^{-k_2 t}) \quad (2)$$

where C_0 is the initial TCB concentration, k_1 and k_2 (h^{-1}) are the average rate constants for HCH and TCB degradation, respectively.

2.6 Analytical methods

Contaminants were extracted from the solid matrix using a Soxhlet. The soils from each column and the reference material were extensively washed by recycling 80 mL of a hexane/acetone mixture (1/1w), for 4 h, in a heated reflux (80°C). The recovered organic phase was reported to 100 mL and diluted if necessary. It was then dehydrated with anhydrous sodium sulphate before analysis. HCH and TCB were analyzed by GC-MS (Perkin Elmer in liquid mode, Restek Rxi-5SilMS 30 m capillary column with 0.25 mm i.d., film thickness 0.25 μm) according to NF EN ISO 6468 and NF EN ISO 10301 standards, respectively. For volatile compounds (DCB, CB and benzene), the analysis was carried out directly on the solid sample by GC-MS in static headspace (Thermo Trace DSQ with PTV injector), by adapting the NF EN ISO 10301 standard. The vial was incubated at 70° for 30 min. Then, 1 mL of the vapor phase was collected (syringe temperature: 77°) and directly injected. Helium was used as a carrier gas with a constant flow rate of 1 $\text{mL} \cdot \text{min}^{-1}$. The quantification limit (QL) of individual compounds (in parentheses) was 4.2 $\mu\text{g} \cdot \text{kg}^{-1}$ (HCH), 33.3 $\mu\text{g} \cdot \text{kg}^{-1}$ (TCB) and 0.01 (1,3-DCB), 0.013 (1,2-DCB), 0.014 (1,4-DCB), 0.01 $\text{mg} \cdot \text{kg}^{-1}$ (CB), respectively. All compounds were identified using analytical standards prepared in methanol. Phenol index was measured by adapting ISO 6439 standard by UV-Vis spectrophotometry (Perkin Elmer Lambda 45) at 510 nm. The QL for the phenol index was 0.5 $\text{mg} \cdot \text{kg}^{-1}$.

3. Theory

The overall rheological behavior of xanthan solutions can be described using the Cross model [57]:

$$\eta = \frac{\eta_0 - \eta_\infty}{(1 + \lambda \dot{\gamma})^m} + \eta_\infty \quad (3)$$

where η_0 and η_∞ are the asymptotic values of viscosity at low and very high shear rates, $\dot{\gamma}$ is the effective shear rate within the porous medium, m measures the degree of dependence of viscosity on the shear rate in the shear-thinning region, while λ is related to the shear rate value where shear-thinning behavior starts (s^{-1}).

The apparent viscosity of the injected solutions in columns η_{app} is defined on the basis of Darcy law:

$$\eta_{app} = \frac{k}{u} \frac{\Delta P}{l} \quad (4)$$

where k is the permeability (m^2), u is the Darcy flow rate ($m.s^{-1}$), ΔP is the pressure drop (Pa) over a length l (m) of a porous medium.

The effective shear-rate within the porous medium ($\dot{\gamma}_{mp}$) is defined according to [58]:

$$\dot{\gamma}_{mp} = \frac{\beta \cdot u}{\sqrt{k} \cdot \varepsilon} \quad (5)$$

where β is a shift factor between the porous medium and bulk and is a function of both the bulk rheology and the porous structure, and ε is the effective porosity of the medium.

4. Results and discussion

4.1 Rheology of xanthan solutions and distribution of alkalinity

4.1.1 Bulk and column measurements

The viscosity of xanthan solutions as a function of the shear-rate are shown in Fig. 2a. An alkalinity-free xanthan solution was used as a reference. Alkalinity has detrimental effects on both viscosity and shear-thinning behavior of the xanthan solutions [59]. This results from the perturbation of the associative behavior of xanthan, which can be attributed to either polymer hydrolysis or lower interpolymer H-bonds density in alkaline medium. Obviously, this perturbation increases in presence of $Ca(OH)_2$ microparticles, nevertheless, the fluid viscosity remains 400-times higher than for pure water.

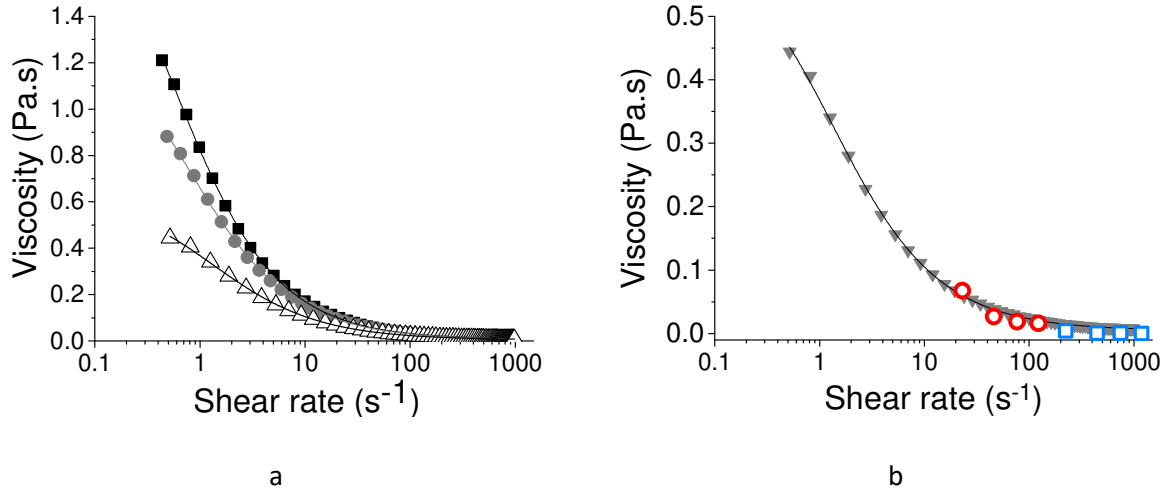


Figure 2. a) Bulk rheology of xanthan (0.2%w) solutions : Xanthan (■), NaOH in xanthan solution (●), Ca(OH)₂ suspensions in xanthan solution (Δ). Lines show fits of experimental data using eq. 3. b) Bulk and porous medium rheologies of the Ca(OH)₂ suspensions in xanthan solution (0.3%/0.2%w). Data from bulk (▼) and soil materials (○ : $k = 9.9 \mu\text{m}^2$ and ○ : $k = 848.7 \mu\text{m}^2$). Pure water viscosity : $8.90 \times 10^{-4} \text{ Pa}\cdot\text{s}$.

The Cross parameters extracted from experimental data, using eq. 3, are presented in Table SM1. The parameters reveal the strong detrimental effect of alkaline amendment on the fluid viscosity at low shear-rates; decreases amounted to 33 and 70% for the NaOH solution and the Ca(OH)₂ suspension in xanthan solution, respectively. However, and most important for injection in soils, the detrimental effect of amendment on viscosity is much lower at high shear-rates. Besides, the shear-thinning behavior starts at lower shear-rates in presence of alkalinity, which is explained by its detrimental effect on polymer association.

The porous medium rheogram obtained from the injections of the Ca(OH)₂ suspension in xanthan solution in soils are shown with the bulk rheogram in Fig. 2b. Those results were obtained using equations 4 and 5 from the pressure gradients measured during the single-step injections in soil-columns (Fig. SM1). A shift factor β of two was used to get the overlap between the two curves. This factor depends on the structure of the porous material, especially on the tortuosity. Values close to the unit were reported for simple materials like uniform glass beads [40,41,60]. However, higher

values (1.7-2.4) were obtained for the injection of amendments, like nZVI, suspended in xanthan solution in sands [61,62]. Nevertheless, shift factors close to one show that the bulk rheological characterization allows the good estimation of pressure gradients in the porous medium [40]. In this study, the rheologies of the $\text{Ca}(\text{OH})_2$ suspension in xanthan solution in bulk and in the soils were similar. This demonstrates that the shear-thinning behavior increases with the shear-rate in these soils. The lower the soil permeability, the higher the shear-rate is, and the lower the fluid viscosity is. For injections in soils, shear-rates were ranging between 20 and 2000 s^{-1} (Fig. 2b) and, as explained above, the detrimental effect of amendment on fluid viscosity is lower at these high rates. Hence, injections should be performed at the highest velocity, being careful to avoid soil fracturing by not exceeding a pressure gradient larger than 0.1 MPa.m^{-1} [63]. The $\text{Ca}(\text{OH})_2$ suspension in xanthan solution can be easily injected because of the moderate pressure gradients recorded. In coarse sand, the injection velocity should be at least 3.8 m.h^{-1} , considering that the recorded pressure gradient was only 0.03 MPa.m^{-1} . However, the injection velocity should be about 1.8 m.h^{-1} in fine sand. Those velocities are common for injections of amendments in the underground [64].

The alkalinity breakthrough curves in fine sand ($k=9.9 \text{ } \mu\text{m}^2$) for NaOH and for $\text{Ca}(\text{OH})_2$ suspension (0.3%, d.: $8 \pm 2 \text{ } \mu\text{m}$) in xanthan solution are shown in Fig. 3a. The plateaus for the relative alkalinity at the output of the column reached the unit after less than 9 PV injected. Obviously, the plateau was reached more rapidly for NaOH, which travelled like a conservative tracer. Fitted values for NaOH using eq. 1' were $(7.1 \pm 0.9) \times 10^{-3} \text{ m}$ for dispersivity and $(6.44 \pm 0.05) \times 10^{-3} \text{ m.s}^{-1}$ for its Darcy-velocity. For $\text{Ca}(\text{OH})_2$, experimental data were analyzed assuming a one-component alkalinity, considering the simplicity of the model and the chi-squared values, and a trapping factor, since the plateaus value of C/C_0 was less than one. The average Darcy velocity for the alkalinity was $(5.11 \pm 0.19) \times 10^{-3} \text{ m.s}^{-1}$, leading to a retardation factor of 1.2 compared with NaOH. Besides, a transmission factor of 91% was calculated for the alkalinity. This demonstrates a fast and high transmission of the alkalinity for the $\text{Ca}(\text{OH})_2$ suspension through this low permeability medium, despite about half was in the solid form as calculated from the solubility product (4.7×10^{-6} at 25°C). This is explained by the fast equilibrium

between the dissolved and the solid forms of Ca(OH)_2 . Yet, a slower release of alkalinity in GW is expected after the injection of the Ca(OH)_2 suspension in the treated zone.

Similar results were reported for the transport of nano and micro ZVI by xanthan solutions using comparable injection velocities [33,40,41,65]. Tiraferri and Sethi [66] have reported the effect of guar gum on the polyaspartate-stabilized nZVI injectability in fine sand. The comparison of the breakthrough curves showed a 3-times improvement for the iron transport in presence of guar gum. However, nZVI accumulated faster at high injection rates, while initial concentrations at the output were higher. The same observation was reported in presence of polyvinylpyrrolidone in columns filled with glass beads [67]. The relative concentration of the transmitted amendment increased by 18-times and was reached 4-times faster. Hence, viscous polymer solutions limit particles aggregation. They also enhance the treatment efficiency in soils, as expected from the increased viscous pressure of xanthan solutions.

After the Ca(OH)_2 transport experiments were performed, the soil columns were sacrificed and the alkalinity was measured in each 2 cm-portions from the input (Fig. 3b). Alkalinity accumulation was observed at the column input. It decreased exponentially with the distance to reach coarsely the value of the injected suspension. This exponential behavior is explained by the balance equation on amendment injection through a filter medium. However, in that case, the observed accumulation only resulted from the delayed transmission of alkalinity, due to the size of the Ca(OH)_2 microparticles. Experimental data were fitted using the following eq. :

$$C/C_0 = A + Be^{(-\kappa x)} \quad (6)$$

where $A = 1.09 \pm 0.072$, $B = 7.80 \pm 0.366$ and $\kappa = 0.176 \pm 0.0125 \text{ cm}^{-1}$ ($R^2 = 0.98$).

The A-value matches perfectly with the transmission factor calculated from the breakthrough curve. Besides, a κ -value of 0.612 cm^{-1} was reported for the transport of nZVI in $4.93 \times 10^{-11} \text{ m}^2$ sand columns [68]. Also, values of 0.364 et 0.260 cm^{-1} were reported for the transmission of nZVI using

pure water and viscous foam, respectively [69], demonstrating that the transport of particles is enhanced for fluids with higher capillary number as expected from fluids with higher viscous force. Despite the size of Ca(OH)_2 microparticles, the κ -values reported in literature were 2 to 4-times larger. The lower retention observed in the present study is explained by the higher viscosity of the xanthan solution (higher fluid capillary number) and because half of the Ca(OH)_2 was dissolved. Similar observations were reported for the transport of iron particles by xanthan solutions [33,60,65]. For the transport of nZVI in glass beads columns and in presence of xanthan (0.3%), the relative iron concentration decreased from 5 to one over a 0.3 m distance [60]. In contrast, the transmission of Ag nanoparticles through sand was very bad when the latter were suspended in pure water [70].

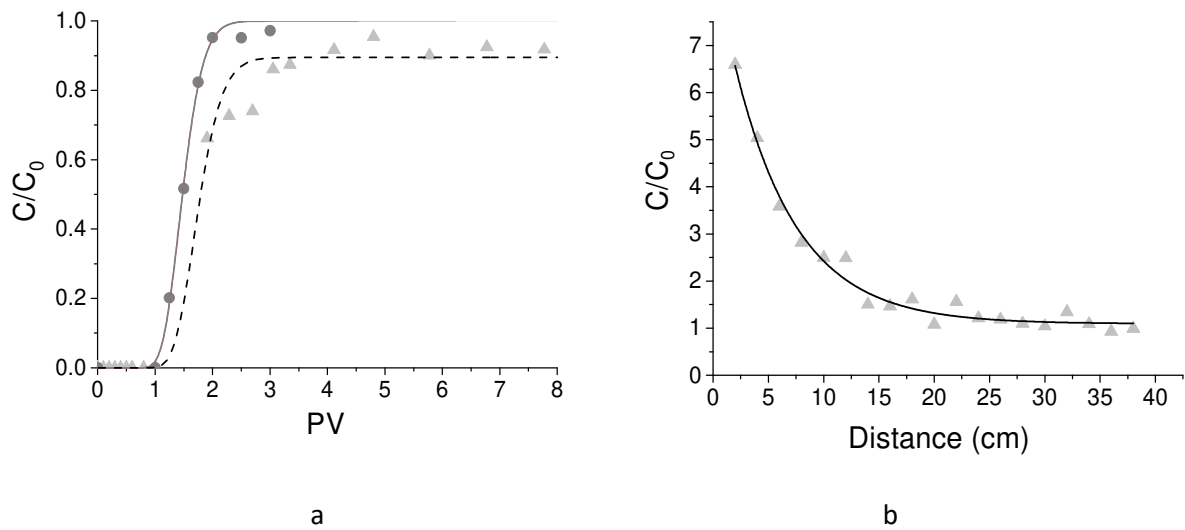


Figure 3. a) Breakthrough curves of alkalinity for NaOH (●, 0.027 M, solid line) and Ca(OH)_2 (▲, 0.3%, dashed line) in xanthan solution (0.2%) in the low permeability ($9.9 \mu\text{m}^2$) contaminated soil column (L: 0.4 m, i.d. 3.5 cm). b) Alkalinity variations along the soil column after transmission measurements for the Ca(OH)_2 suspension in xanthan solution.

4.1.2 Measurements in permeability-contrasted sandbox

Regarding the random and cm-scale variations of the contaminated heterogeneous aquifer, it is impossible to control in which soil permeability the treatment fluid is injected. Therefore, it was decided to study the worst scenario, corresponding to the injection of the treatment fluid in the most permeable material, to see how far the treatment fluid could spread isotropically in the surrounding materials and resist to GW flow. The enhanced distribution and the persistence of alkalinity (pH 12, purple colored) in anisotropic porous medium, under lateral GW flow, using 0.2% xanthan solutions, were studied. The water circulation was used to simulate the GW flow through this REV. A NaOH solution in pure water was used as a reference fluid to compare the behaviors of the dissolved NaOH and the $\text{Ca}(\text{OH})_2$ suspension in xanthan solutions. A longer-lasting alkalinity was expected for the $\text{Ca}(\text{OH})_2$ suspension, because half the alkalinity was in the solid state and its delayed concentration-controlled dissolution. All these alkaline fluids were injected at the back center of the sandbox in a high permeability material (HPM), as shown in Fig. 4. Despite the fact that each fluid mainly propagated in the HPZ, the xanthan-based ones also entered into the surrounding low permeability material (LPM), as previously observed [32,62,71]. Yet, in agreement with its higher shear-thinning behavior, the NaOH in xanthan solution better penetrated the LPM than the $\text{Ca}(\text{OH})_2$ suspension in xanthan solution. Indeed, alkalinity propagated 5- and 7-times faster in the HPM than in the LPM for the NaOH in xanthan solution and the $\text{Ca}(\text{OH})_2$ suspension in xanthan solution, respectively. Besides, in contrast to the alkaline water solution, no fingering was observed during the injection of the viscous xanthan-based fluids, which means a better controlled delivery. Hence, as expected, the increased capillary number of the injected fluids and their shear-thinning behavior allowed to control better viscous fingering and the sweeping of this anisotropic medium.

As shown in Fig. 4, once the injection of alkaline fluids was achieved, the simulated GW flow was colored (red), to study their longevity into the treated zone. In absence of xanthan, only 0.68 PV of GW removed all the injected alkalinity. The resulting solution became blue, corresponding to a pH increase between 10 and 11, because of the fast leaching of alkalinity by the GW flow. In contrast, the GW flow was effectively diverted in the LPM, when xanthan solutions were injected in the HPM.

338 The effectiveness of flow diversion was revealed as a clear inversion of permeability occurred, since
 339 the treated layer became 2.6- and 2.9-times less permeable than the LPM for the $\text{Ca}(\text{OH})_2$ in xanthan
 340 and the NaOH in xanthan fluids, respectively. Hence, the injection of the xanthan solutions produced
 341 a markedly long-lasting blocking effect, which diverted GW flow out of the treated zone. This effect
 342 was also observed for the monitored pH-values at the output of the cell, which displayed a striking
 343 difference associated to the presence of xanthan (Fig. SM3). Whereas a sharp wave of alkalinity with
 344 pH up to 10.4 was observed in absence of xanthan, no significant pH change occurred in its presence.
 345 The strong mobility difference between GW and the xanthan solution is associated to the viscous and
 346 shear-thinning behaviors of the latter. It engenders persistent blocking and GW diverting flow that
 347 ensure the long-lasting activity of the alkaline reagent into the treated zone. A similar blocking
 348 behavior was reported using poly N-isopropylacrylamide, which was attributed to polymer
 349 aggregation blocking the water flow at pores constrictions [72].

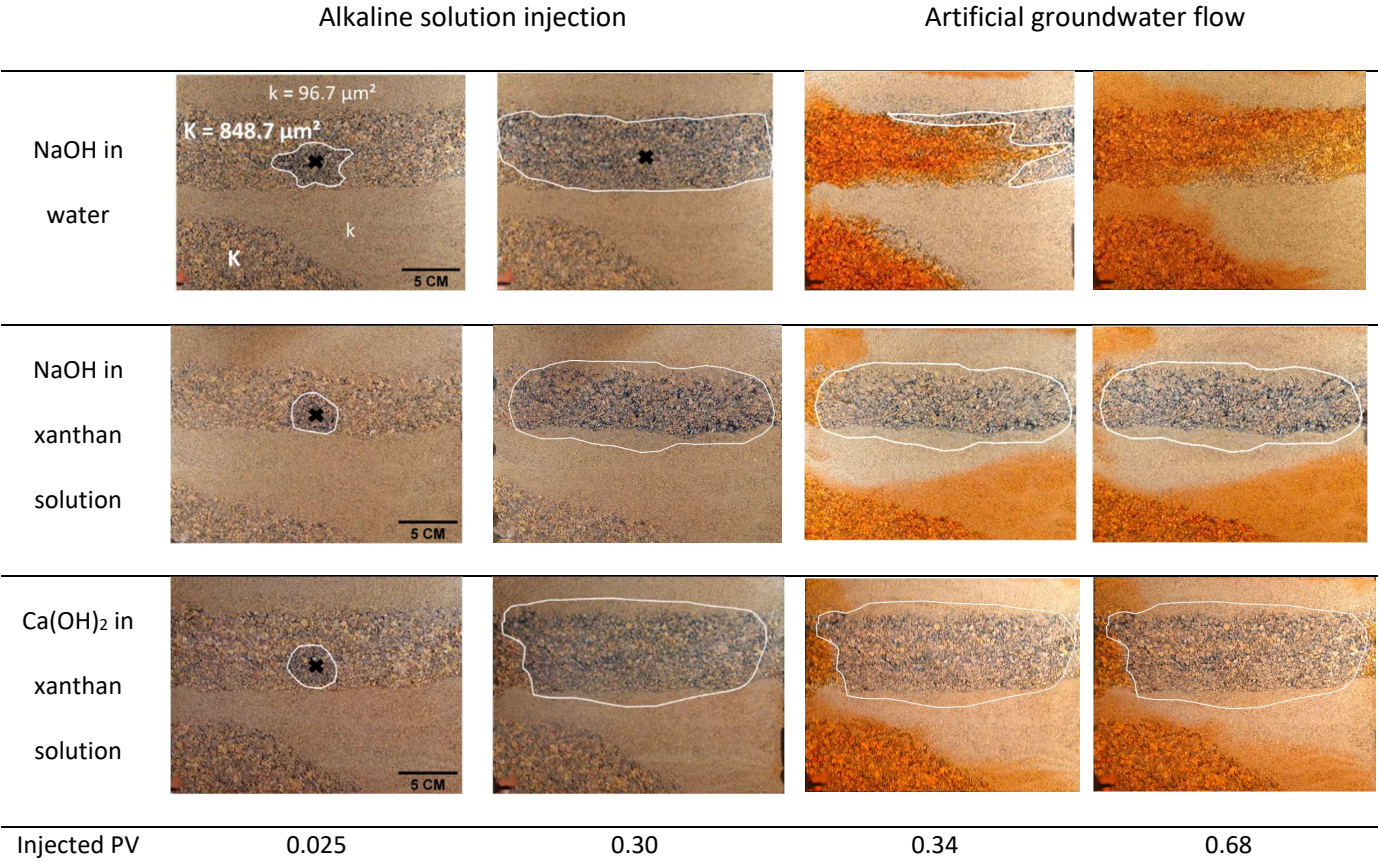


Figure 4. Comparison of alkalinity delivery and lateral sweeping after the delivery of alkalinity in permeability-

contrasted sandbox under water flow (10 m.d^{-1}). The injection process is shown from left to right. The contacted area is delimited by the white solid line.

350

351 The persistence of the Ca(OH)_2 suspension in xanthan solution injected in the HPM was studied over
 352 18 d (Fig.5), which corresponds to more than 150 PV of GW. The model GW was colored after 18 d to
 353 allow a better visualization. Whereas no change could be detected in the treated zone filled with the
 354 Ca(OH)_2 suspension in xanthan solution, the erosion of this viscous gel was observed after 9 d. The
 355 erosion mainly arose in the HPM, both up- and down-stream, with an average $4.6 \times 10^{-3} \text{ m.d}^{-1}$ velocity.
 356 After 18 d, the treated zone was eroded by 20%, however, it remained strongly alkaline despite the
 357 diffusion. Considering the overall permeability of the medium, it felt from 533 to $69 \mu\text{m}^2$ after the
 358 Ca(OH)_2 suspension in xanthan solution was injected. After 18 d, it increased only to $127.3 \mu\text{m}^2$.
 359 These encouraging results suggest that the injection of reactive suspensions and their long-lasting
 360 activity, in strongly permeability-contrasted and high velocity aquifer may be achieved.

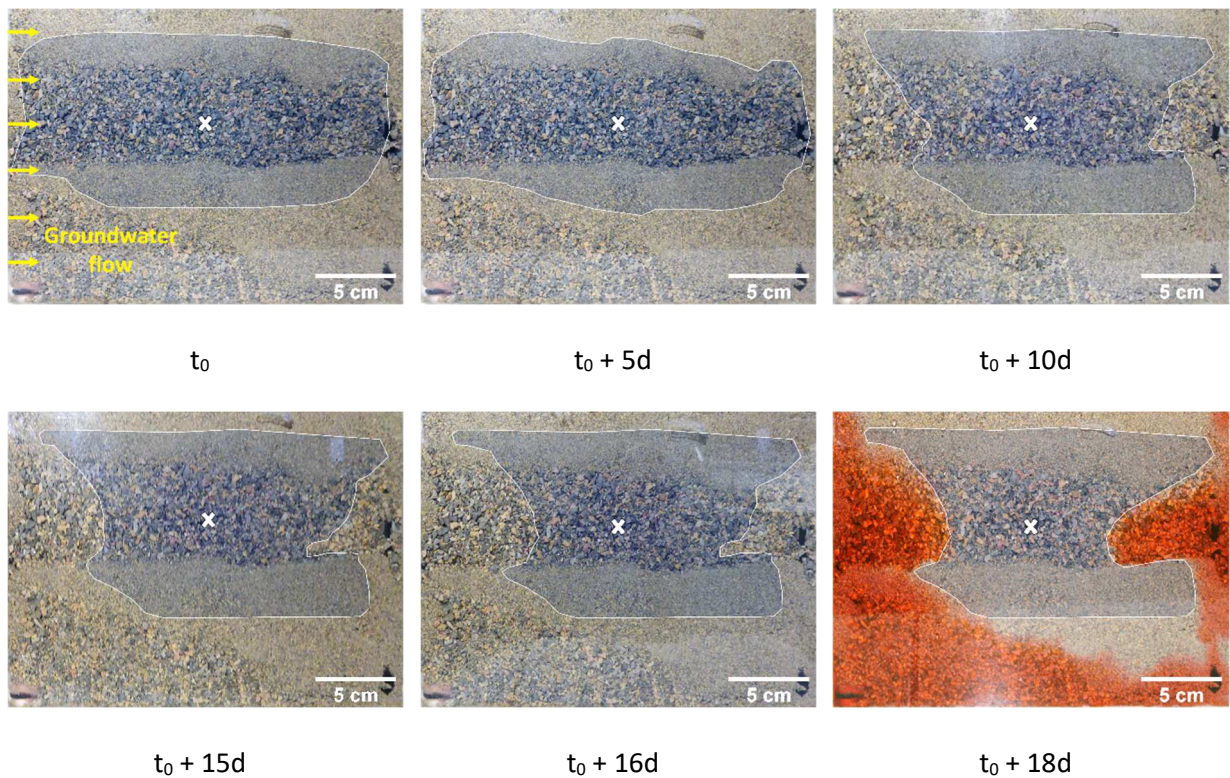


Figure 5. Photographs of lateral sweeping in permeability-contrasted sandbox under water flow (10 m.d⁻¹) after the delivery of a Ca(OH)₂ suspension in xanthan solution in the high permeability zone.

4.2 Kinetics and mechanisms of contaminants degradation

The alkaline degradation of the HCHs and TCBs in the contaminated fine sand (9.9 μm²) was studied once the Ca(OH)₂ suspension in xanthan solution was injected. Degradation kinetics of these COCs present in the contaminated soil were pseudo-first order.

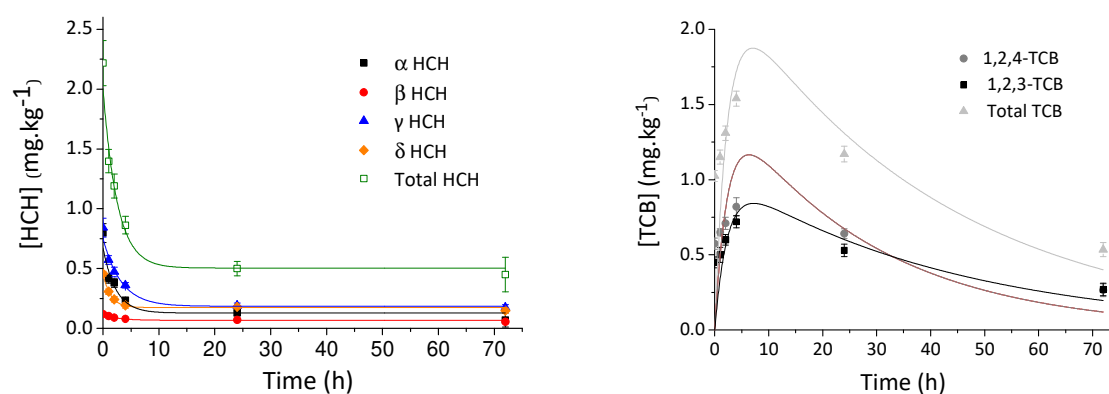


Figure 6. Alkaline degradation kinetics of HCHs (left) and time-dependance of TCBs concentrations (right) in the treated soils using the Ca(OH)₂ suspension in xanthan solution.

Kinetic documents shown in Fig. 6 indicate the fast degradation of HCHs at pH 12 and the production of 1,2,3-TCB and 1,2,4-TCB as metabolites, in agreement with the literature [73,74]. Two HCHs fractions were observed, a readily degradable one and an inert one. The most reactive fraction of HCHs was degraded within 17h regardless their initial concentrations, considering highest initial values of 4.2 mg.kg⁻¹. This is consistent with reported values in aqueous solution for pHs close to 12 [52,73]. As coarsely observed in our experiments, a linear-relationship was found between the logarithm of the rate constant of γ-HCH hydrolysis and the pH, in alkaline solutions [73]. Considering the kinetic documents shown in Fig. 6, the measured pseudo-first order rate-constants were $0.32 \pm$

0.03, 0.12 ± 0.01 , 0.22 ± 0.02 and $0.25 \pm 0.03 \text{ h}^{-1}$ for α , β , γ and δ isomers, respectively. The reactivity of the isomers ranks as $\alpha\text{-HCH} > \delta\text{-HCH} > \gamma\text{-HCH} > \beta\text{-HCH}$, in agreement with the sequence reported in an alkaline ethanol/water solution, whereas the expected order from steric considerations is $\alpha\text{-HCH} > \gamma\text{-HCH} > \delta\text{-HCH} > \beta\text{-HCH}$ [10,52]. Furthermore, the inert fraction of HCHs was minor, but its amount depended strongly on both the isomers and their initial concentrations in soils. For example, for $\gamma\text{-HCH}$, it varied between 7 and 21%, depending on the initial concentrations, but it ranged between 0.2 and 0.3 mg.kg^{-1} . Considering the document in Fig. 6 (left), it amounted to 8.8, 45.8, 20.8 and 32.3 % for α , β , γ and δ isomers, respectively. This order matches quite well their sorption potential, which follows $\gamma\text{-HCH} < \alpha\text{-HCH} < \beta\text{-HCH} < \delta\text{-HCH}$ [10,12].

Regarding the metabolites, 1,2,4-TCB was the major product (57%), followed by 1,2,3-TCB (30%), in agreement with other authors [73,75]. 1,3,5-TCB was detected, but its concentrations were below the QL. Our results suggest a dehydrohalogenation of HCHs to pentachlorocyclohexene (PCCH) followed by TCBs, as previously observed in similar conditions [73,75]. PCCH was identified as intermediate, based on the NIST-library, but not quantified in absence of standard. Yet, tetrachlorocyclohexadienes were not detected. Regarding the risks associated with the production of hazardous metabolites, phenols, hexachlorobenzene, pentachlorobenzene, tetrachlorobenzenes, dibenzodioxins (PCDDs) and polychlorinated dibenzofurans (PCDFs) were systematically sought, but never detected in these conditions. Yet, considering the degradation of concentrated HCHs mixtures in a methanol/water solution at pH 12, the sum of PCDFs amounted to 400 pg.L^{-1} , which represented 10^{-5} % of the mass balance on the HCHs degradation.

After 24 and 72h of reaction, TCBs, DCBs, MCB and benzene were identified as metabolites. However, the last three compounds were below the QL. In contrast to what is reported in pure water, TCBs were not end products [73]. First order degradation rate-constants were 0.023 ± 0.017 and $0.036 \pm 0.021 \text{ h}^{-1}$ for 1,2,3-TCB and 1,2,4-TCB, respectively, and the calculated half-lives amounted to 25h. Even if the mechanism of TCBs degradation is unclear, deacetylation of xanthan

which takes place at $\text{pH} > 9$, may produce an e-donor compound, required for the reductive hydrogenolysis of the chlorobenzenes [76–78]. Furthermore, air-sparging is also effective to remove TCBs from the contaminated GW, given their Henry constants and vapor pressures [79].

5. Conclusion

Xanthan gels were assessed to perform the alkaline dechlorination of HCHs and their TCBs metabolites in a sedimentary aquifer of strong permeability contrast and high velocity. The alkaline degradation was selected because of the low cost of NaOH and $\text{Ca}(\text{OH})_2$. Despite the fact that strong alkalinity and $\text{Ca}(\text{OH})_2$ microparticles have harmful effects on the viscosity of xanthan gels, this property is maintained, and so is their shear-thinning behavior. In contrast to water solution, the alkaline gels have shown a lack of fingering and an enhanced sweeping during their propagation through an anisotropic sandbox with a high permeability contrast. Considering the shear-thinning behavior of the xanthan gels, injections should be performed at a velocity that is as high as possible, while avoiding soil fracturing. Anticipated injection velocities in the field should range from 1.8 to 4 m.h^{-1} , considering the range of soil permeability. Breakthrough curves for the alkaline xanthan solutions carried out in a silty sand demonstrated the fast and high transmission of the alkalinity at low pressure. Injected xanthan gels demonstrated a persistent blocking effect in the treated zone and GW flow diversion. Considering all the results, the use of NaOH in xanthan solution is recommended. Despite the high velocity GW flow, the long-lasting alkalinity in the treated zone matched the degradation of most of HCHs and their TCBs metabolites. Yet, the occurrence of CBs dichlorination in xanthan deserves further study. This shear-thinning gels technology is therefore promising for the ISR of anisotropic aquifers contaminated by slowly desorbing contaminants.

6. Acknowledgments

This research was carried out as a part of the FAMOUS project funded by the French Management Agency of Energy and Environment. The authors acknowledge Sarah Caradec for chemical analysis and Laura Fatin-Rouge for her help to improve the English of the manuscript.

7. References

- [1] A. Chávez, C. Maya, R. Gibson, B. Jiménez, The removal of microorganisms and organic micropollutants from wastewater during infiltration to aquifers after irrigation of farmland in the Tula Valley, Mexico, *Environ. Pollut.* 159 (2011) 1354–1362. doi:10.1016/j.envpol.2011.01.008.
- [2] M. Oteng-Pepurah, M.A. Acheampong, N.K. deVries, Greywater Characteristics, Treatment Systems, Reuse Strategies and User Perception—a Review, *Water. Air. Soil Pollut.* 229 (2018). doi:10.1007/s11270-018-3909-8.
- [3] Commissariat général au développement durable, *L'eau et les milieux aquatiques*, CGDD/SOES. Paris, 2016.
- [4] V. Antoni, *Basol : un panorama des sites et sols pollués, ou potentiellement pollués, nécessitant une action des pouvoirs publics*, Paris, 2013.
- [5] P. Bhatt, M.S. Kumar, T. Chakrabarti, Fate and degradation of POP-hexachlorocyclohexane, *Crit. Rev. Environ. Sci. Technol.* 39 (2009) 655–695. doi:10.1080/10643380701798306.
- [6] J. Vijgen, P.C. Abhilash, Y.F. Li, R. Lal, M. Forter, J. Torres, N. Singh, M. Yunus, C. Tian, A. Schäffer, R. Weber, Hexachlorocyclohexane (HCH) as new Stockholm Convention POPs—a global perspective on the management of Lindane and its waste isomers, *Environ. Sci. Pollut. Res.* 18 (2011) 152–162. doi:10.1007/s11356-010-0417-9.
- [7] J.A. Salam, N. Das, Remediation of lindane from environment - an overview, *Int. J. Adv. Biol. Res.* 2 (2012) 9–15. doi:10.1666/0094-8373(2001)027<0485:AOESGI>2.0.CO;2.

- 449 [8] R. Lal, G. Pandey, P. Sharma, K. Kumari, S. Malhotra, R. Pandey, V. Raina, H.-P.E. Kohler, C.
450 Holliger, C. Jackson, J.G. Oakeshott, Biochemistry of Microbial Degradation of
451 Hexachlorocyclohexane and Prospects for Bioremediation, *Microbiol. Mol. Biol. Rev.* 74 (2010)
452 58–80. doi:10.1128/mmb.00029-09.
- 453 [9] C.M. Dominguez, S. Rodriguez, D. Lorenzo, A. Romero, A. Santos, Degradation of
454 Hexachlorocyclohexanes (HCHs) by Stable Zero Valent Iron (ZVI) Microparticles, *Water. Air.*
455 *Soil Pollut.* 227 (2016). doi:10.1007/s11270-016-3149-8.
- 456 [10] S. Li, D.W. Elliott, S.T. Spear, L. Ma, W.X. Zhang, Hexachlorocyclohexanes in the environment:
457 Mechanisms of dechlorination, *Crit. Rev. Environ. Sci. Technol.* 41 (2011) 1747–1792.
458 doi:10.1080/10643389.2010.481592.
- 459 [11] C.M. Dominguez, A. Romero, A. Santos, Selective removal of chlorinated organic compounds
460 from lindane wastes by combination of nonionic surfactant soil flushing and Fenton oxidation,
461 *Chem. Eng. J.* (2018). doi:10.1016/j.cej.2018.09.170.
- 462 [12] S. Wacławek, D. Silvestri, P. Hrabák, V.V.T. Padil, R. Torres-Mendieta, M. Wacławek, M. Černík,
463 D.D. Dionysiou, Chemical oxidation and reduction of hexachlorocyclohexanes: A review,
464 *Water Res.* 162 (2019) 302–319. doi:10.1016/j.watres.2019.06.072.
- 465 [13] US EPA, *In Situ Treatment Technologies for Contaminated Soil*, 2006.
- 466 [14] A. Muggeridge, A. Cockin, K. Webb, H. Frampton, I. Collins, T. Moulds, P. Salino, Recovery
467 rates, enhanced oil recovery and technological limits, *Philos. Trans. R. Soc. A Math. Phys. Eng.*
468 *Sci.* 372 (2014). doi:10.1098/rsta.2012.0320.
- 469 [15] O. Atteia, E. Del Campo Estrada, H. Bertin, Soil flushing: A review of the origin of efficiency
470 variability, *Rev. Environ. Sci. Biotechnol.* 12 (2013) 379–389. doi:10.1007/s11157-013-9316-0.
- 471 [16] K.R. Reddy, Technical Challenges to In-situ Remediation of Polluted Sites, *Geotech. Geol. Eng.*
472 28 (2010) 211–221. doi:10.1007/s10706-008-9235-y.

- 473 [17] P. Ohrstrom, M. Persson, J. Albergel, P. Zante, S. Nasri, R. Berndtsson, J. Olsson, Field-scale
474 variation of preferential flow as indicated from dye coverage, *J. Hydrol.* 257 (2002) 164–173.
- 475 [18] S.E. Allaire, S. Roulier, A.J. Cessna, Quantifying preferential flow in soils: A review of different
476 techniques, *J. Hydrol.* 378 (2009) 179–204. doi:10.1016/j.jhydrol.2009.08.013.
- 477 [19] Y. Zhang, Z. Zhang, Z. Ma, J. Chen, J. Akbar, S. Zhang, C. Che, M. Zhang, A. Cerdà, A review of
478 preferential water flow in soil science, *Can. J. Soil Sci.* 98 (2018) 604–618. doi:10.1139/cjss-
479 2018-0046.
- 480 [20] I. Bouzid, J. Maire, S.I. Ahmed, N. Fatin-Rouge, Enhanced remedial reagents delivery in
481 unsaturated anisotropic soils using surfactant foam, *Chemosphere.* 210 (2018).
482 doi:10.1016/j.chemosphere.2018.07.081.
- 483 [21] I. Bouzid, J. Maire, N. Fatin-Rouge, Comparative assessment of a foam-based oxidative
484 treatment of hydrocarbon-contaminated unsaturated and anisotropic soils, *Chemosphere.*
485 233 (2019) 667–676. doi:10.1016/j.chemosphere.2019.05.295.
- 486 [22] X. Shen, L. Zhao, Y. Ding, B. Liu, H. Zeng, L. Zhong, X. Li, Foam, a promising vehicle to deliver
487 nanoparticles for vadose zone remediation, *J. Hazard. Mater.* 186 (2011) 1773–1780.
488 doi:10.1016/j.jhazmat.2010.12.071.
- 489 [23] I. Bouzid, D. Pino Herrera, M. Dierick, Y. Pechaud, V. Langlois, P.Y. Klein, J. Albaric, N. Fatin-
490 Rouge, A new foam-based method for the (bio)degradation of hydrocarbons in contaminated
491 vadose zone, *J. Hazard. Mater.* 401 (2021) 123420. doi:10.1016/j.jhazmat.2020.123420.
- 492 [24] D. O'Connor, D. Hou, Y.S. Ok, Y. Song, A.K. Sarmah, X. Li, F.M.G. Tack, Sustainable in situ
493 remediation of recalcitrant organic pollutants in groundwater with controlled release
494 materials: A review, *J. Control. Release.* 283 (2018) 200–213.
495 doi:10.1016/j.jconrel.2018.06.007.
- 496 [25] R. Lenormand, E. Touboul, C. Zarcone, Numerical models and experiments on immiscible

497 displacements in porous media, *J. Fluid Mech.* 189 (1988) 165–187.
 498 doi:10.1017/S0022112088000953.

499 [26] L.W. Lake, Enhanced oil recovery., Prentice Hall Englewood Cliffs, NJ, 1989.

500 [27] D.A.Z. Wever, F. Picchioni, A.. Broekhuis, Polymers for enhanced oil recovery: A paradigm for
 501 structure–property relationship in aqueous solution, *Prog. Polym. Sci.* 36 (2011) 1558–1628.

502 [28] X. Xu, A. Saeedi, K. Liu, An experimental study of combined foam/surfactant polymer (sP)
 503 flooding for carbone dioxide-enhanced oil recovery (CO₂ -EOR), *J. Pet. Sci. Eng.* 149 (2017)
 504 603–611. doi:10.1016/j.petrol.2016.11.022.

505 [29] C. Wei, J. Zheng, L. Xiong, Z. Li, J. Yang, J. Zhang, S. Lin, L. Zhou, L. Fang, Y. Ding, Evaluation and
 506 utilization of nano-micron polymer plug for heterogeneous carbonate reservoir with thief
 507 zones, *Adv. Polym. Technol.* 2020 (2020). doi:10.1155/2020/3498583.

508 [30] K.S. Sorbie, R.S. Seright, P. Recovery, Gel Placement in Heterogeneous Systems With
 509 Crossflow, in: SPE, Society of Petroleum Engineers, Tulsa, Oklahoma, 1992: p. 369.
 510 doi:https://doi.org/10.2118/24192-MS.

511 [31] T. Tosco, F. Gastone, R. Sethi, Guar gum solutions for improved delivery of iron particles in
 512 porous media (Part 2): Iron transport tests and modeling in radial geometry, *J. Contam.*
 513 *Hydrol.* 166 (2014) 34–51. doi:10.1016/j.jconhyd.2014.06.014.

514 [32] L. Zhong, M. Oostrom, M.J. Truex, V.R. Vermeul, J.E. Szecsody, Rheological behavior of
 515 xanthan gum solution related to shear thinning fluid delivery for subsurface remediation, *J.*
 516 *Hazard. Mater.* 244–245 (2013) 160–170. doi:10.1016/j.jhazmat.2012.11.028.

517 [33] J. Xin, F. Tang, X. Zheng, H. Shao, O. Kolditz, Transport and retention of xanthan gum-
 518 stabilized microscale zero-valent iron particles in saturated porous media, *Water Res.* 88
 519 (2016) 199–206. doi:10.1016/j.watres.2015.10.005.

- 520 [34] J. Xin, J. Han, X. Zheng, H. Shao, O. Kolditz, Mechanism insights into enhanced
521 trichloroethylene removal using xanthan gum-modified microscale zero-valent iron particles,
522 J. Environ. Manage. 150 (2015) 420–426. doi:10.1016/j.jenvman.2014.12.022.
- 523 [35] S.C. Hauswirth, P.S. Birak, S.C. Rylander, C.T. Miller, Mobilization of manufactured gas plant
524 tar with alkaline flushing solutions, Environ. Sci. Technol. 46 (2012) 426–433.
525 doi:10.1021/es202278s.
- 526 [36] I. Bouzid, J. Maire, N. Fatin-rouge, Comparative assessment of a foam-based method for ISCO
527 of coal tar contaminated unsaturated soils, J. Environ. Chem. Eng. 7 (2019) 103346.
528 doi:10.1016/j.jece.2019.103346.
- 529 [37] J. Maire, A. Coyer, N. Fatin-rouge, Surfactant foam technology for in situ removal of heavy
530 chlorinated, J. Hazard. Mater. 299 (2015) 630–638. doi:10.1016/j.jhazmat.2015.07.071.
- 531 [38] J. Maire, A. Joubert, D. Kaifas, T. Invernizzi, J. Marduel, S. Colombano, D. Cazaux, C. Marion, P.
532 Klein, A. Dumestre, N. Fatin-rouge, Assessment of flushing methods for the removal of heavy
533 chlorinated compounds DNAPL in an alluvial aquifer, Sci. Total Environ. 612 (2018) 1149–
534 1158. doi:10.1016/j.scitotenv.2017.08.309.
- 535 [39] J. Maire, N. Fatin-Rouge, Surfactant foam flushing for in situ removal of DNAPLs in shallow
536 soils, J. Hazard. Mater. 321 (2017) 247–255. doi:10.1016/j.jhazmat.2016.09.017.
- 537 [40] F. Gastone, T. Tosco, R. Sethi, Guar gum solutions for improved delivery of iron particles in
538 porous media (Part 1): Porous medium rheology and guar gum-induced clogging, J. Contam.
539 Hydrol. 166 (2014) 23–33. doi:10.1016/j.jconhyd.2014.06.013.
- 540 [41] S. Comba, D. Dalmazzo, E. Santagata, R. Sethi, Rheological characterization of xanthan
541 suspensions of nanoscale iron for injection in porous media, J. Hazard. Mater. 185 (2011)
542 598–605. doi:10.1016/j.jhazmat.2010.09.060.
- 543 [42] K.E. Martel, R. Martel, R. Lefebvre, P.J. Gélinas, Laboratory Study of Polymer Solutions Used

544 for Mobility Control During In Situ NAPL Recovery, *Groundw. Monit. Remediat.* (1998) 103–
545 113. doi:<https://doi.org/10.1111/j.1745-6592.1998.tb00734.x>.

546 [43] M. Usman, O. Tascone, P. Faure, K. Hanna, Chemical oxidation of hexachlorocyclohexanes
547 (HCHs) in contaminated soils, *Sci. Total Environ.* 476–477 (2014) 434–439.
548 doi:10.1016/j.scitotenv.2014.01.027.

549 [44] R. García-Cervilla, A. Santos, A. Romero, D. Lorenzo, Remediation of soil contaminated by
550 lindane wastes using alkaline activated persulfate: Kinetic model, *Chem. Eng. J.* 393 (2020)
551 124646.

552 [45] C.M. Dominguez, A. Romero, D. Lorenzo, A. Santos, Thermally activated persulfate for the
553 chemical oxidation of chlorinated organic compounds in groundwater, *J. Environ. Manage.*
554 261 (2020) 110240. doi:10.1016/j.jenvman.2020.110240.

555 [46] B. Karn, T. Kuiken, M. Otto, Nanotechnology and in situ remediation: A review of the benefits
556 and potential risks, *Environ. Health Perspect.* 117 (2009) 1823–1831.
557 doi:10.1289/ehp.0900793.

558 [47] P. Oprčkal, A. Mladenovič, J. Vidmar, A. Mauko Pranjić, R. Milačič, J. Ščančar, Critical
559 evaluation of the use of different nanoscale zero-valent iron particles for the treatment of
560 effluent water from a small biological wastewater treatment plant, *Chem. Eng. J.* 321 (2017)
561 20–30.

562 [48] H. Wang, S. Cai, L. Shan, M. Zhuang, N. Li, G. Quan, J. Yan, Adsorptive and reductive removal
563 of chlorophenol from wastewater by biomass-derived mesoporous carbon-supported sulfide
564 nanoscale zerovalent iron, *Nanomaterials.* 9 (2019) 1–12. doi:10.3390/nano9121786.

565 [49] D. Lorenzo, R. García-Cervilla, A. Romero, A. Santos, Partitioning of chlorinated organic
566 compounds from dense non-aqueous phase liquids and contaminated soils from lindane
567 production wastes to the aqueous phase, *Chemosphere.* 239 (2020) 124798.

- doi:10.1016/j.chemosphere.2019.124798.
- [50] P. Österreicher-Cunha, T. Langenbach, J.P.M. Torres, A.L.C. Lima, T.M.P. De Campos, E.D.A. Vargas, A.R. Wagener, HCH distribution and microbial parameters after liming of a heavily contaminated soil in Rio de Janeiro, *Environ. Res.* 93 (2003) 316–327. doi:10.1016/S0013-9351(03)00091-4.
- [51] J.P.M. Torres, C.I.R. Fróes-Asmus, R. Weber, J.M.H. Vijgen, HCH contamination from former pesticide production in Brazil-a challenge for the Stockholm Convention implementation, *Environ. Sci. Pollut. Res.* 20 (2013) 1951–1957. doi:10.1007/s11356-012-1089-4.
- [52] S. Cristol, The kinetics of the alkaline dehydrochlorination of the benzene hexachloride isomers. The mechanism of second-order elimination reactions., *J. Am. Chem. Soc.* 69 (1947) 338–342.
- [53] I. Watson, A. Burnett, *Hydrology: an Environmental Approach*, 1st Editio, CRC Press, 1995. doi:https://doi.org/10.1201/9780203751442.
- [54] M. Fireman, Permeability Measurements On Disturbed Soil Samples, *Soil Sci.* 58 (1944) 337–354.
- [55] M. Carter, E. Gregorich, *Soil sampling and methods of analysis*, 2nd editio, 2007. doi:https://doi.org/10.1201/9781420005271.
- [56] A. Ogata, R.B. Banks, A solution of the differential equation of longitudinal dispersion in porous media, *Geol. Surv. (U.S.); Prof. Pap.* (1961) A1–A7. <http://pubs.er.usgs.gov/publication/pp411A>.
- [57] M.M. Cross, Rheology of non-Newtonian fluids: A new flow equation for pseudoplastic systems, *J. Colloid Sci.* 20 (1965) 417–437. doi:10.1016/0095-8522(65)90022-X.
- [58] G. Chauveteau, Rodlike Polymer Solution Flow through Fine Pores: Influence of Pore Size on

591 Rheological Behavior, *J. Rheol.* (N. Y. N. Y). 26 (1982) 111–142. doi:10.1122/1.549660.

592 [59] J.J. Sheng, Critical review of alkaline-polymer flooding, *J. Pet. Explor. Prod. Technol.* 7 (2017)

593 147–153. doi:10.1007/s13202-016-0239-5.

594 [60] T. Tosco, R. Sethi, Transport of non-newtonian suspensions of highly concentrated micro- and

595 nanoscale iron particles in porous media: A modeling approach, *Environ. Sci. Technol.* 44

596 (2010) 9062–9068. doi:10.1021/es100868n.

597 [61] L. Ren, J. Dong, Z. Chi, Y. Li, Y. Zhao, E. Jianan, Rheology modification of reduced graphene

598 oxide based nanoscale zero valent iron (nZVI/rGO) using xanthan gum (XG): Stability and

599 transport in saturated porous media, *Colloids Surfaces A Physicochem. Eng. Asp.* 562 (2019)

600 34–41. doi:10.1016/j.colsurfa.2018.11.013.

601 [62] L. Zhong, M. Oostrom, T.W. Wietsma, M.A. Covert, Enhanced remedial amendment delivery

602 through fluid viscosity modifications: Experiments and numerical simulations, *J. Contam.*

603 *Hydrol.* 101 (2008) 29–41. doi:10.1016/j.jconhyd.2008.07.007.

604 [63] US EPA, Hydraulic fracturing technology, EPA 540-R-93-505. (1993) 140.

605 [64] J. Maire, E. Brunol, N. Fatin-Rouge, Shear-thinning fluids for gravity and anisotropy mitigation

606 during soil remediation in the vadose zone, *Chemosphere.* 197 (2018) 661–669.

607 doi:10.1016/j.chemosphere.2018.01.101.

608 [65] E. Dalla Vecchia, M. Luna, R. Sethi, Transport in porous media of highly concentrated iron

609 micro- and nanoparticles in the presence of xanthan gum, *Environ. Sci. Technol.* 43 (2009)

610 8942–8947. doi:10.1021/es901897d.

611 [66] A. Tiraferri, R. Sethi, Enhanced transport of zerovalent iron nanoparticles in saturated porous

612 media by guar gum, *J. Nanoparticle Res.* 11 (2009) 635–645. doi:10.1007/s11051-008-9405-0.

613 [67] B. Liang, Y. Xie, Z. Fang, E.P. Tsang, Assessment of the transport of polyvinylpyrrolidone-

614 stabilised zero-valent iron nanoparticles in a silica sand medium, *J. Nanoparticle Res.* 16
615 (2014). doi:10.1007/s11051-014-2485-0.

616 [68] L. Shi, J. Chen, Q. Wang, X. Song, Effects of carrier on the transport and DDT removal
617 performance of nano-zerovalent iron in packed sands, *Chemosphere*. 209 (2018) 489–495.
618 doi:10.1016/j.chemosphere.2018.06.123.

619 [69] Y. Ding, B. Liu, X. Shen, L. Zhong, X. Li, Foam-Assisted Delivery of Nanoscale Zero Valent Iron in
620 Porous Media, *J. Environ. Eng.* 139 (2013) 1206–1212. doi:10.1061/(ASCE)EE.1943-
621 7870.0000727.

622 [70] Y. Liang, S.A. Bradford, J. Simunek, M. Heggen, H. Vereecken, E. Klumpp, Retention and
623 remobilization of stabilized silver nanoparticles in an undisturbed loamy sand soil, *Environ.*
624 *Sci. Technol.* 47 (2013) 12229–12237. doi:10.1021/es402046u.

625 [71] T. Robert, R. Martel, S.H. Conrad, R. Lefebvre, U. Gabriel, Visualization of TCE recovery
626 mechanisms using surfactant-polymer solutions in a two-dimensional heterogeneous sand
627 model, *J. Contam. Hydrol.* 86 (2006) 3–31. doi:10.1016/j.jconhyd.2006.02.013.

628 [72] A. Tran-Viet, A. F. Routh, A. W. Woods, Control of the Permeability of a Porous Media Using a
629 Thermally Sensitive Polymer, *AIChE J.* 60 (2014). doi:10.1002/aic.14352.

630 [73] X. Liu, P. Peng, J. Fu, W. Huang, Effects of FeS on the transformation kinetics of lindane,
631 *Environ. Sci. Technol.* 43 (2003) 1062–1067.

632 [74] A. Santos, J. Fernandez, S. Rodriguez, C.M. Dominguez, M.A. Lominchar, D. Lorenzo, A.
633 Romero, Abatement of chlorinated compounds in groundwater contaminated by HCH wastes
634 using ISCO with alkali activated persulfate, *Sci. Total Environ.* 615 (2018) 1070–1077.
635 doi:10.1016/j.scitotenv.2017.09.224.

636 [75] A. Santos, J. Fernández, J. Guadaño, D. Lorenzo, A. Romero, Chlorinated organic compounds in
637 liquid wastes (DNAPL) from lindane production dumped in landfills in Sabiñanigo (Spain),

638 Environ. Pollut. 242 (2018) 1616–1624. doi:10.1016/j.envpol.2018.07.117.

639 [76] E.P. Pinto, L. Furlan, C.T. Vendruscolo, Chemical deacetylation natural xanthan
640 (Jungbunzlauer®), Polimeros. 21 (2011) 47–52. doi:10.1590/S0104-14282011005000005.




641 [77] J. He, Y. Sung, M.E. Dollhopf, B.Z. Fathepure, J.M. Tiedje, F.E. Löffler, Acetate versus hydrogen
642 as direct electron donors to stimulate the microbial reductive dechlorination process at
643 chloroethene-contaminated sites, Environ. Sci. Technol. 36 (2002) 3945–3952.
644 doi:10.1021/es025528d.

645 [78] F. BRAHUSHI, F.O. KENGARA, Y. SONG, X. JIANG, J.C. MUNCH, F. WANG, Fate Processes of
646 Chlorobenzenes in Soil and Potential Remediation Strategies: A Review, Pedosphere. 27
647 (2017) 407–420. doi:10.1016/S1002-0160(17)60338-2.

648 [79] Agency for Toxic Substances and Disease Registry, Trichlorobenzenes, (2019).
649 <https://www.atsdr.cdc.gov/ToxProfiles/tp.asp?id=1168&tid=255#bookmark08> (accessed June
650 25, 2020).

651

652

-  Contaminated zone
-  Alkaline polymer solution
-  Groundwater flow

